Materials Transactions, Vol. 49, No. 6 (2008) pp. 1401 to 1409

Nucleation of the Primary Al Phase on $TiAl_3$ during Solidification in Hot-Dip Zn-11%Al-3%Mg-0.2%Si-Coated Steel Sheet*[1]

Kazuhiko Honda[1], Kohsaku Ushioda[1,*2], Wataru Yamada[1], Koki Tanaka[2] and Hidetoshi Hatanaka[3]

[1]*Kimitsu R&D Lab, Technical Development Bureau, Nippon Steel Corp., Kimitsu 299-1141, Japan*
[2]*Advanced Technology Research Lab, Technical Development Bureau, Nippon Steel Corp., Futtsu 293-8511, Japan*
[3]*Kimitsu Works, Nippon Steel Corp., Kimitsu 299-1141, Japan*

The solidification structure of a hot-dip Zn-11%Al-3%Mg-0.2%Si coated steel sheet with a slight Ti addition was investigated by EBSD. In every center of the primary Al phase of the alloy-coating layer, $TiAl_3$ was observed by a scanning electron microscope, which suggests that $TiAl_3$ acts as a heterogeneous nucleation site of the primary Al phase. The latter was revealed to have perfect lattice coherency with the nucleus $TiAl_3$ phase. The crystal orientation relationships between $TiAl_3$ and the primary Al are $(001)_{TiAl_3}$ // $(001)_{Al}$ and $[100]_{TiAl_3}$ // $[100]_{Al}$, $(100)_{TiAl_3}$ // $(001)_{Al}$ and $[001]_{TiAl_3}$ // $[100]_{Al}$, $(102)_{TiAl_3}$ // $(110)_{Al}$ and $[\bar{2}01]_{TiAl_3}$ // $[\bar{1}10]_{Al}$, $(110)_{TiAl_3}$ // $(110)_{Al}$ and $[\bar{1}10]_{TiAl_3}$ // $[\bar{1}10]_{Al}$, indicating that the primary Al phase grows in an epitaxial manner from the nucleus $TiAl_3$ phase. The planar disregistry δ between the two phases was calculated to be less than 5%, owing to this good lattice coherency. The $TiAl_3$ phase is considered to decrease the degree of undercooling necessary for the nucleation of the primary Al phase. [doi:10.2320/matertrans.MRA2008010]

(Received January 9, 2008; Accepted March 12, 2008; Published April 23, 2008)

Keywords: *zinc-aluminium-magnesium-silicon alloy-coated steel sheet, aluminium, titanium aluminium alloy, nucleation, electron back scattering diffraction pattern, lattice coherency, planar disregistry*

1. Introduction

Hot-dip galvanized steel sheets are widely used in the markets of construction, electrical appliances, and so on, since they have good corrosion resistance. Particularly in the field of construction, where materials are subjected to a severe outdoor corrosion environment, Zn-5 mass%Al[1)] and 55 mass%Al-Zn[2)] alloy-coated steel sheets have been practically used with corrosion resistance improved owing to the addition of Al. Recently, hot-dip Zn-Al-Mg alloy-coated steel sheets with the further corrosion resistance have been developed and the volume of steels used is soaring.[3–6)]

Zn-Al and Zn-Al-Mg alloys exhibit eutectic reactions and Al dendrite is formed as the primary crystal when the Al content is hypereutectic. Since the size of the primary Al phase depends on the cooling rate, crystal refinement is expected to be controlled by changing the degree of undercooling.

It is well known that the injection of particles, such as $TiAl_3$, TiB_2 and TiC, has the effect of crystal refinement in the cast Al alloys,[7)] although no research has been reported on whether or not a similar effect is expected for the crystal refinement of the primary Al during the hot-dip process.

In this paper, the addition of Ti to a coating bath with composition of Zn-11 mass%Al-3 mass%Mg-0.2 mass%Si was studied in terms of the crystal refinement of the primary Al. Emphasis was placed upon discussion of the mechanism.

2. Experimental Procedure

The coating test was carried out using a hot-dip galvanizing simulator, as shown in Fig. 1. A steel sheet of thickness of 0.8 mm was first reheated to 1053 K for 60 s in an atmosphere of N_2 with 3 vol% H_2, which resulted in a reduction in the surface of the specimen. Subsequently the specimen was cooled to 773 K in the same atmosphere and dipped in a molten bath of 723 K for 3 s followed by N_2 wiping, which controlled the coating thickness to within 70∼90 g/m^2 followed by gas cooling to room temperature.

The two types of coating bath, namely the Zn bath with the additions of 11 mass%Al-3 mass%Mg-0.2 mass%Si and the Zn bath with the further addition of 100 mass ppm Ti, were used.

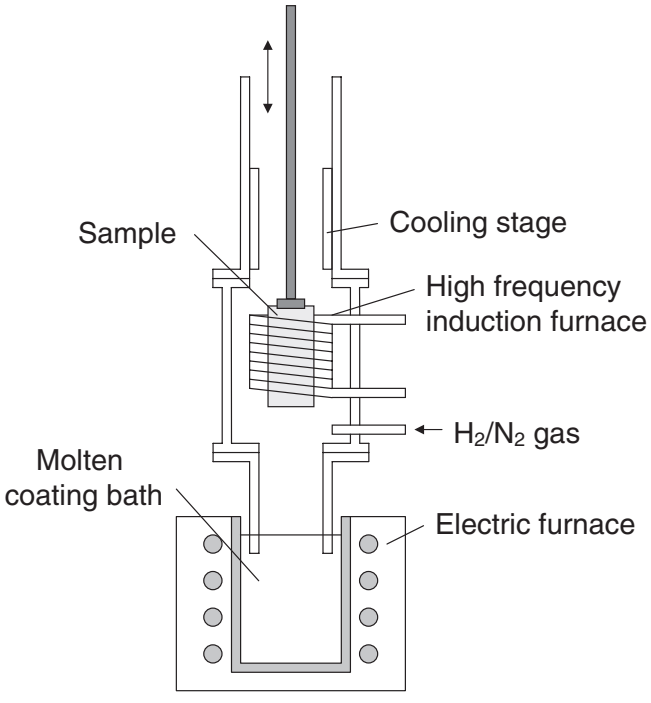

Fig. 1 Schematic view of galvanizing simulator.

*[1]This Paper was Originally Published in Japanese in J. Japan Inst. Metals **72** (2008) 43–50.
*[2]Present address: Technical Development Bureau, Nippon Steel Corp.

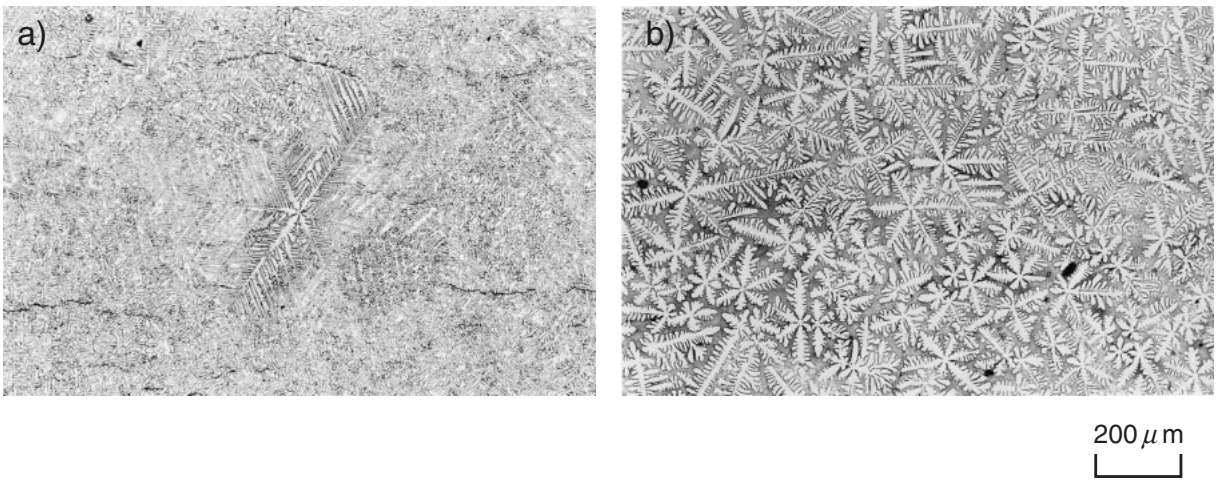

Fig. 2 Optical micrographs showing dendrite structures at the top surface of Zn-11 mass%Al-3 mass%Mg-0.2 mass%Si coating, a) without Ti addition, and b) with Ti addition.

The solidification structure was observed by optical microscopy after polishing the surface layer from the top surface followed by etching with nital reagents and EBSD (Electron Back Scattering Diffraction Pattern) was used for the crystal orientation analysis. The specimen was chemically polished and subjected to high resolution scanning electron microscopy, while crystal orientation analysis using EBSD was carried out by FE-SEM (Hitachi S-4300SE) with an EBSD detector and TSL software.

In the primary Al phase of Zn-11 mass%Al-3 mass%Mg-0.2 mass%Si just after solidification commenced, significant amounts of Zn were contained, whereas at low temperatures, the primary Al phase is decomposed into two phases, namely the Al and Zn phases, due to a monotectoid reaction.[8] Consequently, it may be possible that the lattice constant of the Al phase at high temperature differs from that in low temperature. With this in mind, the lattice constant of the Al phase with Zn in a solid solution was measured using the high temperature X-ray diffractometer, M18XCE, produced by McScience.

3. Experimental Results

3.1 Solidification structure of Zn-11 mass%Al-3 mass%Mg-0.2 mass%Si

The optical micrographs of the solidification structure of the coating layer in Zn-11 mass%Al-3 mass%Mg-0.2 mass%-Si are shown in Fig. 2, together with that of the coating layer with the Ti addition. It is clear that the Ti addition refined the dendrite structure of the primary Al phase.

Figure 3 shows the result of EPMA analysis for the primary Al phase in the coating layer of the Ti added Zn-11 mass%Al-3 mass%Mg-0.2 mass%Si steel sheets. In every center of the Al dendrites, intermetallic compounds were observed, which were revealed to include both Ti and Al by EPMA element mapping. Therefore, this intermetallic compound was implied to be that of the Ti-Al series.

3.2 High temperature X-ray diffraction

Figure 4 shows the calculated quasi-equilibrium phase diagram of the Zn-Al-Mg alloy series with 3 mass%Mg using Thermo-Calc.[9] Since the Zn-11 mass%Al-3 mass%Mg alloy contains Al as a hypereutectic, it is clear that the Al phase crystallizes first as the primary, followed by an eutectic reaction, which leads to the Al and $MgZn_2$ phases. Finally, the solidification is completed by a ternary eutectic reaction, resulting in the Zn, Al and $MgZn_2$ phases. The calculated change in compositions as a function of temperature in the Al phase of Zn-11 mass%Al-3 mass%Mg alloy is shown in Fig. 5. The calculation using Themo-Calc clarifies that the primary Al phase contains as much as 40 mass%Zn at the temperature where solidification commences.

In order to measure the lattice constant of the crystallizing primary Al phase with so much Zn, high temperature X-ray diffraction was carried out using a specially prepared Al-40 mass%Zn alloy. According to the phase diagram of Al-Zn alloy, Al-40 mass%Zn alloy at room temperature is decomposed into two phases, namely the Al and Zn phases, due to the monotectoid reaction. However at temperatures exceeding 623 K, only the Al phase with Zn in solid solution exists. Therefore high temperature X-ray diffraction was performed at 703 K, close to the completion temperature of solidification of the Al-40 mass%Zn alloy.

Figure 6 shows the results of X-ray diffraction of Al-40 mass%Zn alloy; both at room temperature and 703 K. The fact that only the diffraction peak of the Al phase was detected at 703 K indicates that Zn is completely in a solid solution in the Al phase at 703 K. Furthermore, the measured lattice constants, as determined by the $\cos^2\theta$extrapolation method using diffraction peaks, are 0.4048 nm at room temperature and 0.4086 nm at 703 K, respectively. The lattice constant at 703 K is about 0.004 nm larger than that at room temperature. Therefore the result allows us to infer that the lattice constant at the temperature where solidification commences is slightly larger than that at room temperature. Since the difference is a maximum of 1%, the discussion on lattice coherency in the next chapter was carried out using the lattice constant described in JCPDS card in the sense that the lattice constant in the solidification temperature range may be approximated by that at room temperature.

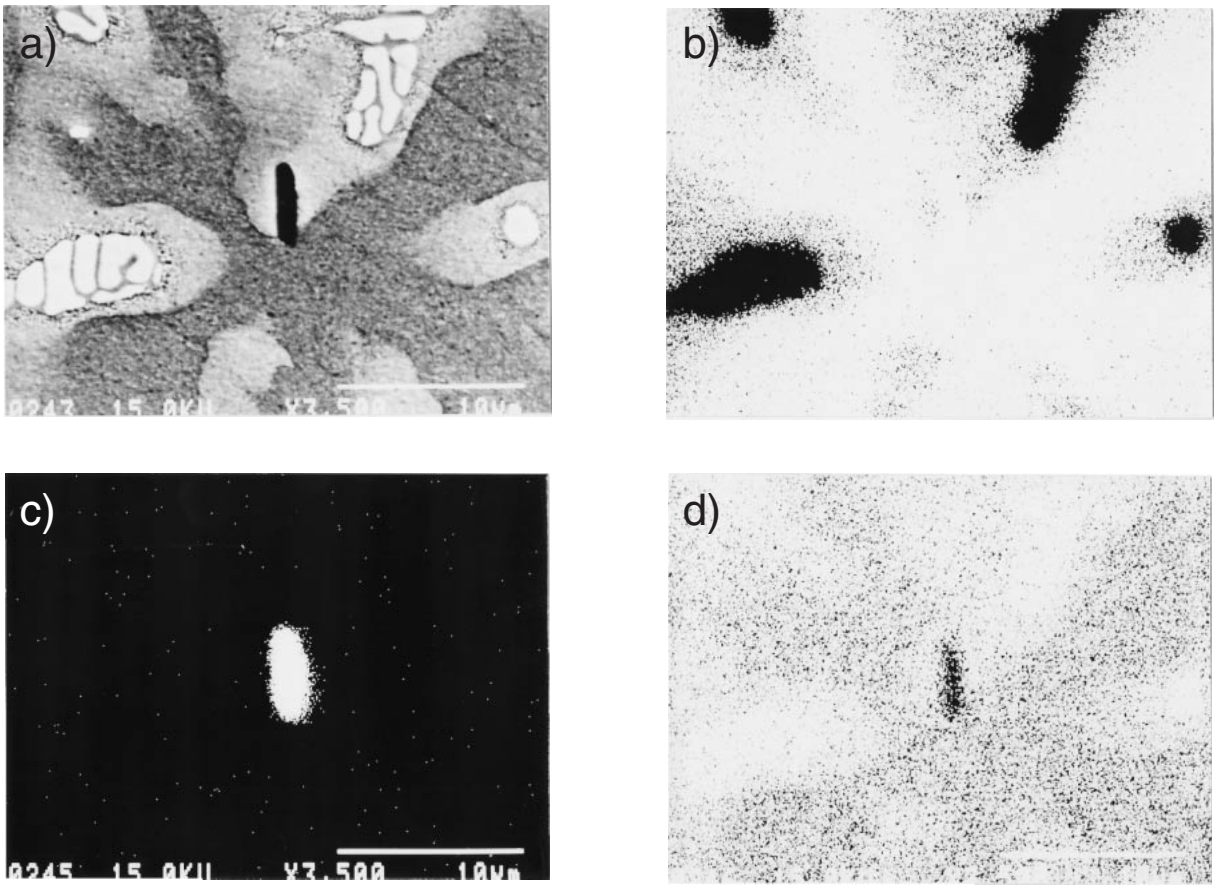

Fig. 3 X-ray images by EPMA showing the Ti-Al intermetallic compound in the center of the Al dendrite in Zn-11 mass%Al-3 mass%Mg-0.2 mass%Si coating with 100 mass ppm Ti addition. a) SE image, b) Al, c) Ti, d) Zn.

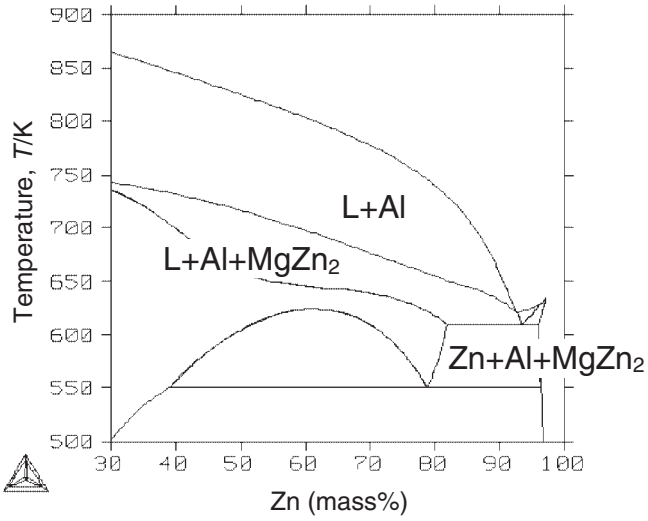

Fig. 4 Calculated metastable phase diagram of the Zn-Al-Mg system at 3 mass%Mg.

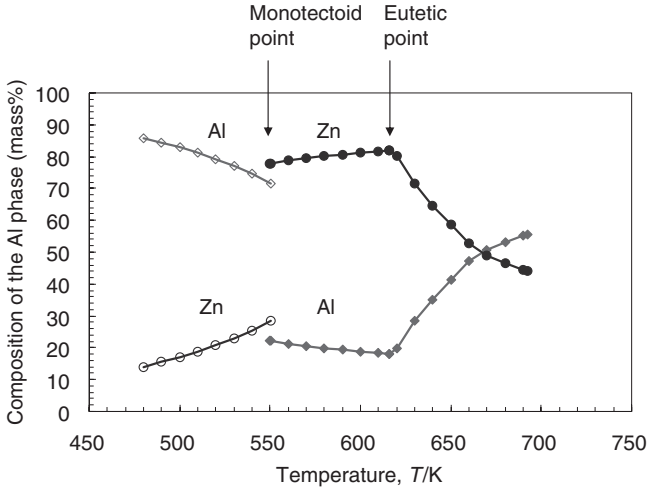

Fig. 5 Calculated change in compositions of the Al phase in Zn-11 mass%Al-3 mass%Mg alloy.

Moreover, the intermetallic compound $TiAl_3$ was newly prepared and subjected to high temperature X-ray diffraction to measure the lattice constant, since the Ti-Al intermetallic compound in the primary Al confirmed by EPMA was considered to be $TiAl_3$. Figure 7 shows the results of X-ray diffraction of $TiAl_3$, both at room temperature and 723 K. Almost no difference in the angle of the diffracted peak was observed. Furthermore the measured lattice constants determined by the $\cos^2\theta$ extrapolation method using diffraction peaks are 0.3875 nm in a-axis and 0.8616 nm in c-axis at room temperature, and 0.3895 nm in a-axis and 0.8666 nm in c-axis at 723 K, respectively. Again the difference in the lattice constants between 723 K and room temperature are as little as about 0.002 nm in a-axis and about 0.005 nm in

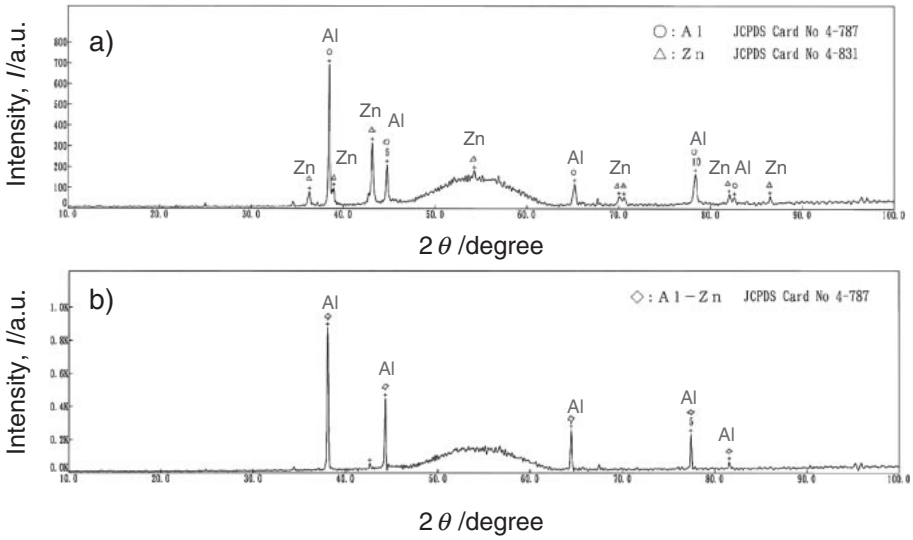

Fig. 6 X-ray diffraction patterns of Al-40 mass%Zn alloy, measured at a) RT, and b) 703 K.

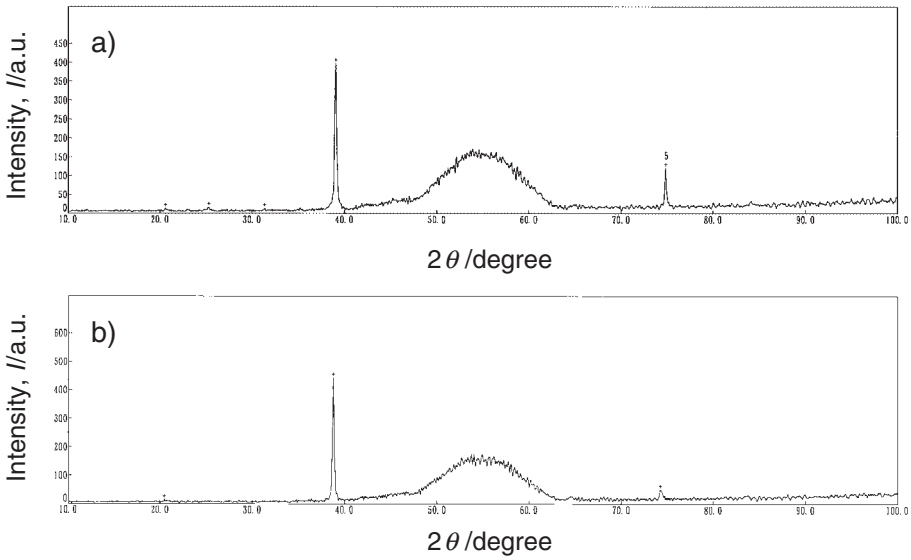

Fig. 7 X-ray diffraction patterns of $TiAl_3$, measured at a) RT, and b) 723 K.

c-axis. Therefore, the later discussion, relating to the lattice coherency, was performed using the lattice constant described in the JCPDS card, assuming the lattice constant in the solidification temperature range to be almost the same as that at room temperature.

3.3 EBSD analysis

Figure 8 shows the results of EBSD of the coating layer in Zn-11 mass%Al-3 mass%Mg-0.2 mass%Si with Ti addition. As already demonstrated in Fig. 4, during the hot-dip coating of Zn-11 mass%Al-3 mass%Mg-0.2 mass%Si, the Al phase crystallizes first as the primary, through the eutectoids of the Al and $MgZn_2$ phases, before the solidification is finally completed by the ternary eutectic reaction; resulting in the Zn, Al and $MgZn_2$ phases. Therefore, the orientation mapping of the Al phase in Fig. 8 shows that of the primary Al phase, whereas the orientation mapping of the Zn phase shows that of the Zn phase comprising the ternary eutectic structure.

The orientation mapping image of the Al phase reveals that dendrites with {001} orientation, parallel to the sheet surface in the solidification structure, are spread in four directions, whereas dendrites with {111} orientation are spread in six directions. It has been reported that in the case of Al-Zn alloy with high Zn content, the dendrite of the Al phase easily grows in the ⟨110⟩ direction.[10] Taking into consideration the fact that Al belongs to FCC metal, the dendrites in the solidification structure are expected to grow in four and six directions when the primary Al crystals have {001} and {111} orientations parallel to sheet surface, respectively. As shown in Fig. 8, exactly the expected structures were observed.

Moreover, Fig. 8 indicates that every dendrite of the primary Al phase has its own unique orientation, which implies that the orientation information of the primary Al phase is inherited to the Al phase, even after the monotectoid reaction takes place, because the primary Al phase formed during solidification is decomposed into the Al and Zn phase

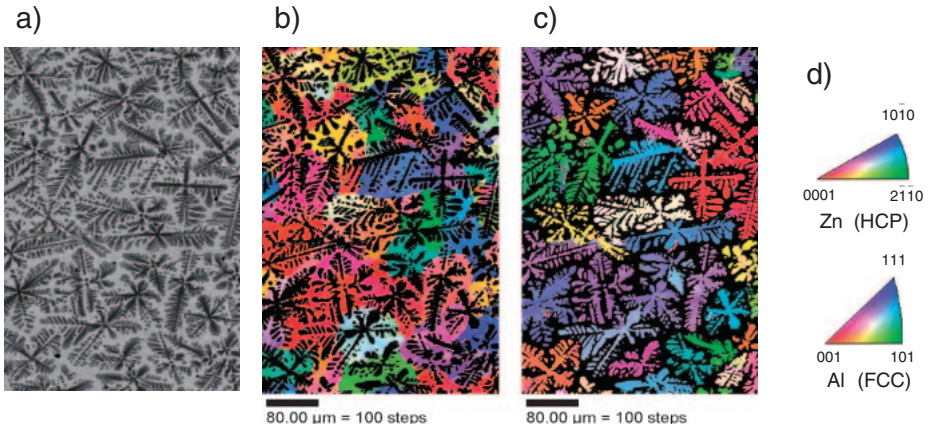

Fig. 8 BSE image and EBSD orientation mapping, showing the solidified structure of Zn-11 mass%Al-3 mass%Mg-0.2 mass%Si coating with 100 mass ppm Ti addition. a) BSE image, b) orientation mapping image of Zn, c) orientation mapping image of Al, d) stereo triangles of Zn (HCP) and Al (FCC) showing color-indicated orientations.

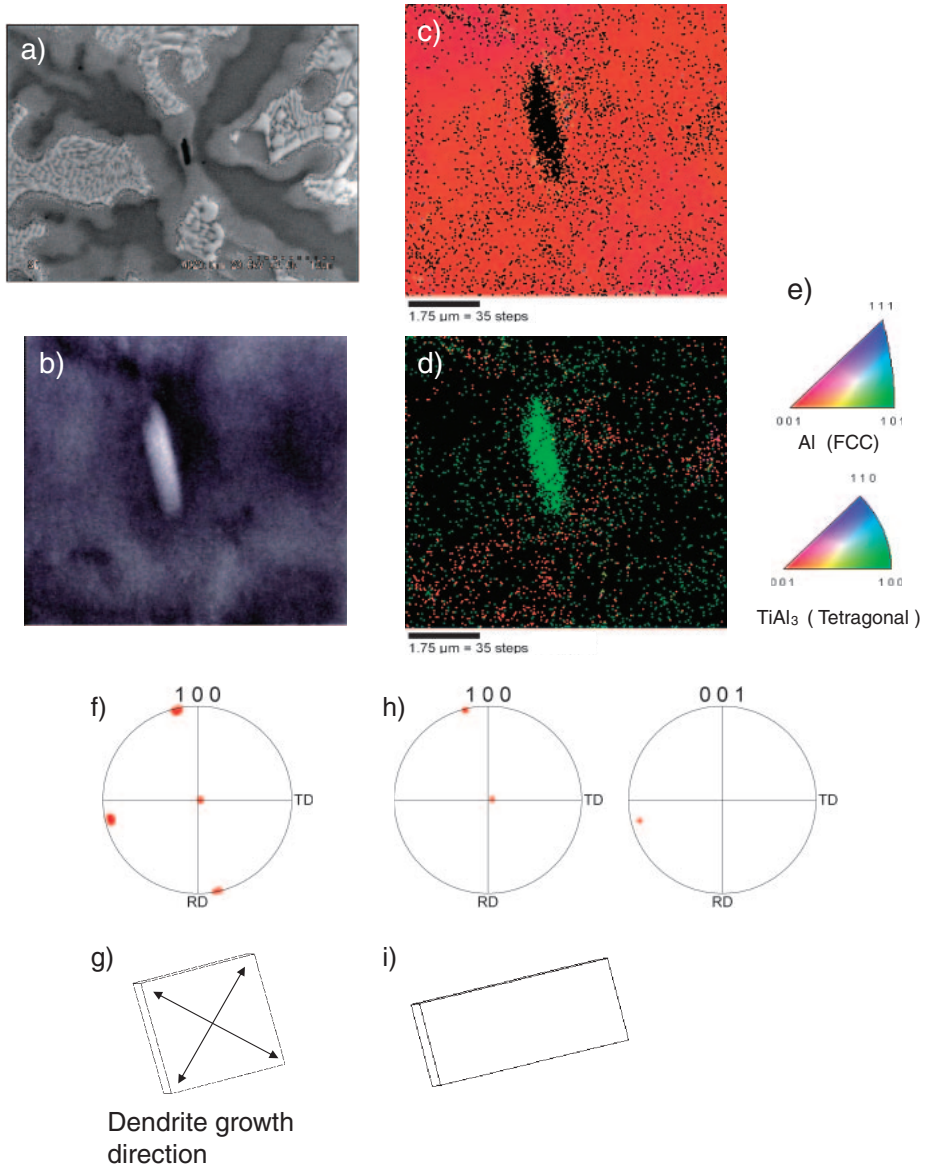

Fig. 9 BSE image and EBSD orientation mapping showing $TiAl_3$ in Al dendrite. a) BSE image of Al dendrite, b) enlarged BSE image of a), c) orientation mapping of Al, d) orientation mapping of $TiAl_3$, e) stereo triangles of Al (FCC) and $TiAl_3$ (Tetragonal), f) {100} pole figure of Al dendrite, g) crystal orientation of Al dendrite, h) {100} pole figure and {001} pole figure of $TiAl_3$ and i) crystal orientation of $TiAl_3$.

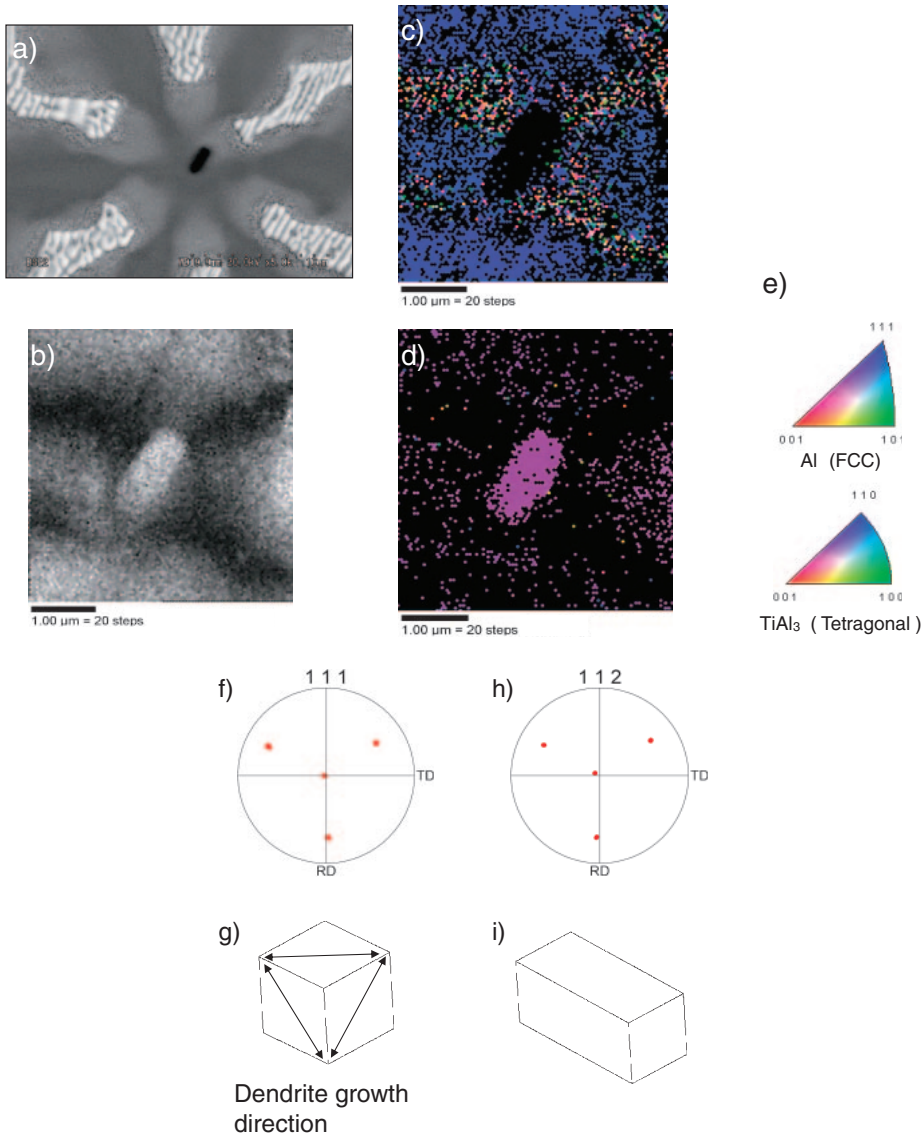

Fig. 10 BSE image and EBSD orientation mapping showing $TiAl_3$ in Al dendrite. a) BSE image of Al dendrite, b) enlarged BSE image of a), c) orientation mapping of Al, d) orientation mapping of $TiAl_3$, e) stereo triangles of Al (FCC) and $TiAl_3$ (Tetragonal), f) {111} pole figure of Al dendrite, g) crystal orientation of Al dendrite, h) {112} pole figure of $TiAl_3$ and i) crystal orientation of $TiAl_3$.

due to the monotectoid reaction.[8] Therefore, the orientation map of the Al phase in Fig. 8 may be considered to be that of the primary Al phase.

Figure 9 shows the EBSD results on the nucleus of the primary Al phase, which has the {001} plane parallel to the sheet (polished) surface. The dendrite of the Al phase with {001} plane was initially selected, whereupon the EBSD patterns were obtained from the center of the dendrites. As indicated in the SEM image in Fig. 9(a) and (b), in the center of the dendrites the intermetallic compounds, presumably $TiAl_3$, were observed and the EBSD patterns from these intermetallic compounds have excellent agreement with those from the artificially prepared $TiAl_3$. The crystal orientations of $TiAl_3$ thus indexed were revealed to have a {100} plane parallel to the sheet surface as shown in Fig. 9(d). The pole figures of Al and $TiAl_3$ are shown in Fig. 9(f) and (h), whereas the crystal models inferred from the pole figures are described in Fig. 9(g) and (i). The crystal orientations of Al and $TiAl_3$ are parallel in the sense that not only the polished surfaces but also the other planes perpendicular to {100} are parallel. Therefore, the crystal orientation of $TiAl_3$ perfectly accords in three dimensions with that of Al, which preferentially nucleated on $TiAl_3$. Moreover, the dendrite growth direction of Al was confirmed to be ⟨110⟩.

Figure 10 shows the result of EBSD analysis where the Al phase has the {111} plane parallel to the sheet (polished) surface. The EBSD measurement was carried out in the dendrite center of the Al phase. The SEM image in Fig. 10(a) shows $TiAl_3$ in the dendrite center and here, the polished surface of $TiAl_3$ was revealed to have a {112} plane. Pole figures of Al and $TiAl_3$ are shown in Fig. 10(f) and (h), whereas the crystal models inferred from the pole figures are described in Fig. 10(g) and (i). The crystal orientations of Al and $TiAl_3$ are parallel in the sense that not only the polished surfaces but also all other {111} planes are parallel to all {112} planes of $TiAl_3$. Therefore, the crystal orientation of $TiAl_3$ perfectly accords in three dimensions with that of Al,

which nucleated on $TiAl_3$. Moreover, again in this case, the dendrite of the Al phase was confirmed to grow into a ⟨110⟩ direction.

The pole of one dendrite of the Al phase in Figs. 9(f) and 10(f) was relatively broad, which is considered to stem from the fact that the Al phase in the dendrite is comprised of numerous and very fine Al crystals due to the monotectoid reaction of the primary Al.

4. Discussion

Figure 11 shows the unit cells of the crystal structure for Al and $TiAl_3$. Al has an FCC structure, whereas $TiAl_3$ has a $D0_{22}$ structure. Since the $D0_{22}$ structure of $TiAl_3$ is characterized by the points whereby 1) two Al unit cells (FCC) are piled and 2) An Al atom in the four corners and the center are substituted by the Ti atom, the unit cell of $TiAl_3$ significantly resembles that of Al. Moreover, taking into account the fact that the lattice constants are in very close proximity, we can presume the lattice coherency for various planes of Al and $TiAl_3$ to be essentially excellent.

Figure 12(a) and (b) show the superimposed atomic arrangements between the $(001)_{Al}$ and $(001)_{TiAl_3}$ planes, and $(100)_{Al}$ and $(100)_{TiAl_3}$ planes. Figure 13(a) and (b) show the case between $(101)_{Al}$ and $(102)_{TiAl_3}$ planes, and $(110)_{Al}$ and $(110)_{TiAl_3}$ planes. Furthermore the calculated planer disregistries (δ) in terms of lattice incoherency for these planes are listed in Table 1. Here, δ was calculated using eq. (1),[11] which takes into account the difference in angle caused by the atomic arrangements of materials belonging to different crystal structures.

$$\delta^{(hkl)_s}_{(hkl)_n} = \sum_{i=1}^{3} \frac{\dfrac{|d[uvw]^i_s \cos\theta_1 - d[uvw]^i_n|}{d[uvw]^i_n}}{3} \times 100, \qquad (1)$$

where $(hkl)_s$: plane with low index of $TiAl_3$, $[uvw]_s$: normal direction of $(hkl)_s$ plane, $(hkl)_n$: plane with low index of Al, $[uvw]_n$: normal direction of $(hkl)_n$ plane, $d[uvw]_s$: atomic distance in the direction of $[uvw]_s$, $d[uvw]_n$: atomic distance in the direction of $[uvw]_n$, θ_1: angle between $[uvw]_s$ and $[uvw]_n$.

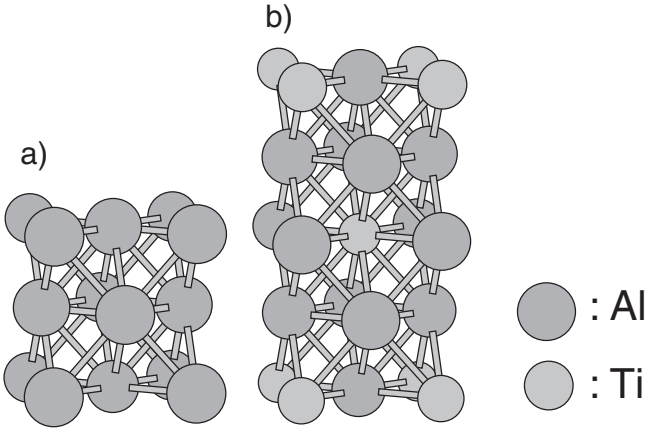

Fig. 11 Unit cell of a) Al (FCC), b) $TiAl_3$ ($D0_{22}$).

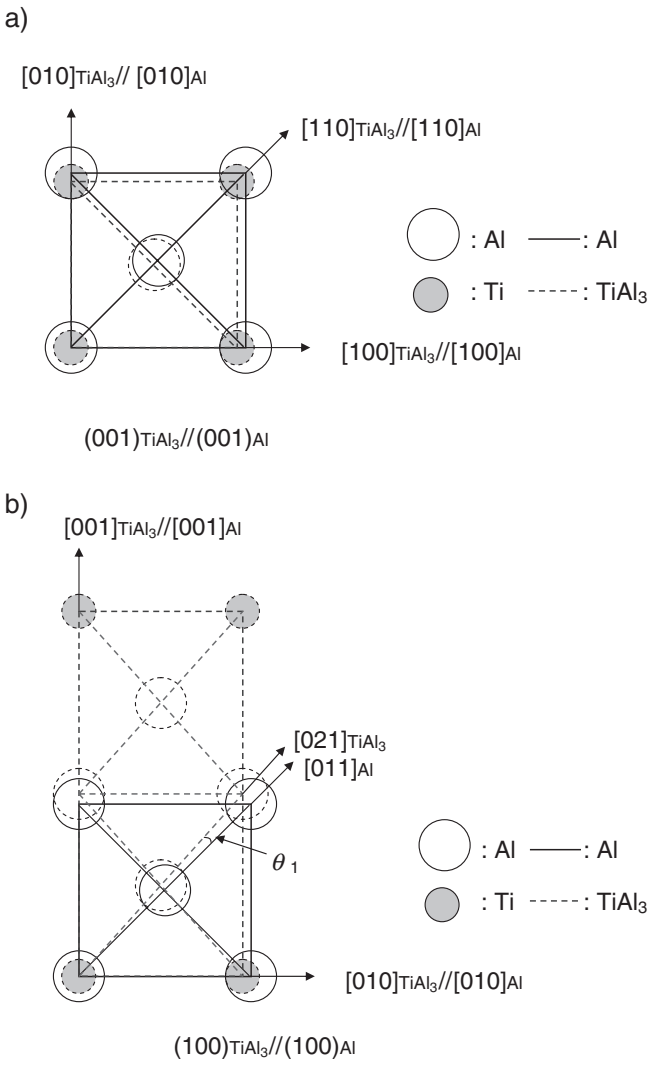

Fig. 12 Schematic superimposed presentation of atomic arrangements of a) between $(001)_{TiAl_3}$ and $(001)_{Al}$ with 4.8% misfit and $\theta_1 = 0°$, and b) between $(100)_{TiAl_3}$ and $(100)_{Al}$ with 3.6% misfit and $\theta_1 = 2.8°$.

It is clear that the disregistries (δ) of $(100)_{TiAl_3}$ // $(001)_{Al}$, $(001)_{TiAl_3}$ // $(001)_{Al}$, $(110)_{TiAl_3}$ // $(110)_{Al}$, and $(102)_{TiAl_3}$ // $(110)_{Al}$ are less than 5% and considered to be small enough in terms of lattice coherency, which is one of the most important factors controlling the capability for heterogeneous nucleus.

Moreover, according to the EBSD results shown in Figs. 9 and 10, the following orientation relationships between $TiAl_3$ and Al are confirmed; $(001)_{TiAl_3}$ // $(001)_{Al}$ and $[100]_{TiAl_3}$ // $[100]_{Al}$, $(100)_{TiAl_3}$ // $(001)_{Al}$ and $[\bar{2}01]_{TiAl_3}$ // $[\bar{1}10]_{Al}$, $(102)_{TiAl_3}$ // $(\bar{1}10)_{Al}$ and $[\bar{2}01]_{TiAl_3}$ // $[\bar{1}10]_{Al}$, $(110)_{TiAl_3}$ // $(110)_{Al}$ and $[\bar{1}10]_{TiAl_3}$ // $[\bar{1}10]_{Al}$, which indicate that the primary Al phase grows in an epitaxial manner from the nucleus $TiAl_3$ phase. In other words, the epitaxial growth of the primary Al phase on $TiAl_3$ takes place very easily. This is presumably associated with the fact that the simple substitution of Ti atoms by Al atoms leads to the change from $TiAl_3$ to Al, due to the excellent lattice coherency and the closeness of unit cells between Al and $TiAl_3$.

Consequently the reason why the Ti addition to the coating bath with Zn-11 mass%Al-3 mass%Mg-0.2 mass%Si resulted

Table 1 Planar disregistry between $TiAl_3$ and Al.

Plane form	$[uvw]_s$	$[uvw]_n$	$d[uvw]_s$	$d[uvw]_n$	θ_1 (deg)	$\delta^{(hkl)_s}_{(hkl)_n}$
$(001)_{TiAl_3}$ // $(001)_{Al}$	$[100]_{TiAl_3}$	$[100]_{Al}$	3.854	4.049	0	4.8
	$[110]_{TiAl_3}$	$[110]_{Al}$	2.725	2.862	0	
	$[010]_{TiAl_3}$	$[010]_{Al}$	3.854	4.049	0	
$(100)_{TiAl_3}$ // $(100)_{Al}$	$[010]_{TiAl_3}$	$[010]_{Al}$	3.854	4.049	0	3.6
	$[021]_{TiAl_3}$	$[011]_{Al}$	2.868	2.862	2.8	
	$[001]_{TiAl_3}$	$[001]_{Al}$	8.584	4.049	0	
$(102)_{TiAl_3}$ // $(101)_{Al}$	$[\bar{2}01]_{TiAl_3}$	$[\bar{1}01]_{Al}$	2.868	2.862	0	2.2
	$[\bar{2}21]_{TiAl_3}$	$[\bar{1}11]_{Al}$	2.301	2.338	1.5	
	$[010]_{TiAl_3}$	$[010]_{Al}$	3.854	4.049	0	
$(110)_{TiAl_3}$ // $(110)_{Al}$	$[\bar{1}10]_{TiAl_3}$	$[\bar{1}10]_{Al}$	2.725	2.862	0	4.2
	$[\bar{2}21]_{TiAl_3}$	$[\bar{1}11]_{Al}$	2.301	2.338	2.6	
	$[001]_{TiAl_3}$	$[001]_{Al}$	8.584	4.049	0	

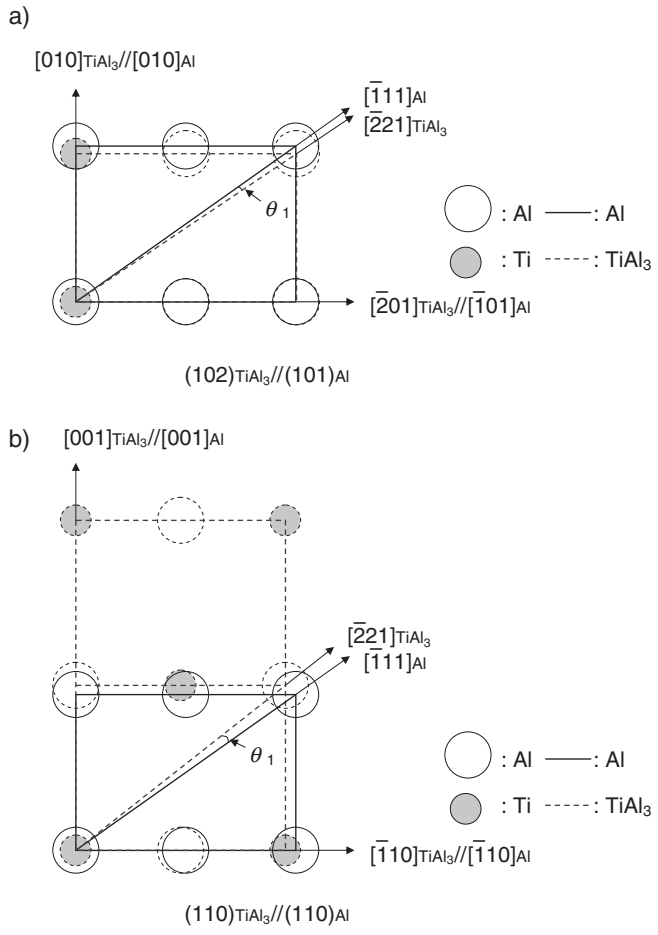

Fig. 13 Schematic superimposed presentation of atomic arrangements of a) between $(102)_{TiAl_3}$ and $(101)_{Al}$ with 2.2% misfit and $\theta_1 = 1.5°$, and b) between $(110)_{TiAl_3}$ and $(110)_{Al}$ with 4.2% misfit and $\theta_1 = 2.6°$.

in the refinement of the Al phase may be considered to stem from the fact that $TiAl_3$, which initially crystallizes in the molten bath, acts as the preferential nucleation site of the primary Al. Namely, the $TiAl_3$ phase is considered to decrease the degree of undercooling necessary for the heterogeneous nucleation of the primary Al.

According to the EBSD results in Figs. 9 and 10, the dendrites of the Al phase are considered to grow into the ⟨110⟩ direction. Gonzales *et al.*[10] reported that the Al dendrite growth direction in Zn-Al solution is determined by the interface energy between the liquid and the Al crystal, and the Al dendrite, when containing more than 60 mass%Zn, grows into the ⟨110⟩ direction. This is in positive agreement with the present experimental result.

In the early stage of solidification Al grows in an epitaxial manner on $TiAl_3$, however, after it grows to a certain size, the Al dendrite is considered to grow into the ⟨110⟩ direction. This is because the growth direction is determined by minimizing the total energy, supposedly by the interfacial energy between liquid and Al, under circumstances where the primary Al surrounds $TiAl_3$ and the interface between the liquid and Al becomes dominant.

5. Conclusion

The solidification structure of a hot-dip Zn-11 mass%Al-3 mass%Mg-0.2 mass%Si coated steel sheet with a small amount of Ti addition was investigated and the following conclusions were obtained:

(1) As for the solidification structure of a hot-dip Zn-11 mass%Al-3 mass%Mg-0.2 mass%Si, the primary Al phase is refined by the Ti addition.

(2) In every center of the primary Al phase of the alloy-coating layer with Ti addition, $TiAl_3$ was observed.

(3) The primary Al phase contains as much as 40 mass%Zn in solid solution, however, the lattice constant at the solidification temperature range is almost the same as that at room temperature.

(4) EBSD analysis revealed that the crystal orientation of $TiAl_3$ in Al phase perfectly accords with that of the surrounding Al phase. The crystal orientation relationships between $TiAl_3$ and primary Al are $(001)_{TiAl_3}$ // $(001)_{Al}$ and $[100]_{TiAl_3}$ // $[100]_{Al}$, $(100)_{TiAl_3}$ // $(001)_{Al}$ and $[001]_{TiAl_3}$ // $[100]_{Al}$, $(102)_{TiAl_3}$ // $(110)_{Al}$ and $[\bar{2}01]_{TiAl_3}$ // $[\bar{1}10]_{Al}$, $(110)_{TiAl_3}$ // $(110)_{Al}$ and $[\bar{1}10]_{TiAl_3}$ // $[\bar{1}10]_{Al}$, indicating that the primary Al phase grows in an epitaxial manner from the nucleus $TiAl_3$ phase.

(5) The planar disregistry δ between the Al and $TiAl_3$ phases was calculated to be less than 5%. Owing to the excellent lattice coherency, the $TiAl_3$ phase is consid-

ered to decrease the degree of undercooling necessary for the heterogeneous nucleation of the primary Al phase.

(6) Consequently the Ti addition into the coating bath with Zn-11 mass%Al-3 mass%Mg-0.2 mass%Si is considered to make the $TiAl_3$ phase crystallize first in liquid, which acts as the heterogeneous nucleation sites of the Al phase, resulting in a solidification structure with a relatively equiaxed and fine primary Al phase.

Acknowledgements

To conduct this study, we acknowledge Emeritus Prof. M. Maki of Kyoto University (presently Executive Advisor of Nippon Steel Corp.), Profs. Y. Mishima and M. Kato of Tokyo Institute of Technology and Dr. M. Sugiyama of Nippon Steel Corp. for thoughtful guidance. In measurement of EBSD, we appreciate the cooperation of Mr. K. Yamaguchi of Ishikawa Metal Finishing Corp.

REFERENCES

1) K. Tano, J. Oka, M. Kamada and M. Obu: J. Surf. Finish. Soc. Jpn. **33** (1982) 516.
2) D. J. Blickwede: Tetsu-to-Hagane **66** (1980) 821.
3) A. Komatsu, H. Izutani, T. Tsujimura, A. Andoh and T. Kittaka: Tetsu-to-Hagane **86** (2000) 534.
4) T. Tsujimura, A. Komatsu and A. Andoh: Proc. 5th Int. Conf. on Zinc and Zinc Alloy Coated Steel Sheet (Galvatech '01), Verlag Stahleisen GmbH, Düsseldorf, (2001) 145.
5) S. Tanaka, K. Honda, A. Takahashi, Y. Morimoto, M. Kurosaki, H. Shindo, K. Nishimura and M. Sugiyama: Proc. 5th Int. Conf. on Zinc and Zinc Alloy Coated Steel Sheet (Galvatech '01), Verlag Stahleisen GmbH, Düsseldorf, (2001) 153.
6) Y. Morimoto, M. Kurosaki, K. Honda, K. Nishimura, S. Tanaka, A. Takahashi and H. Shindo: Tetsu-to-Hagane **89** (2003) 161.
7) A. Kamio: J. JILM **52** (2002) 479.
8) K. Honda and W. Yamada: Collected Abstracts of the 2007 Spring Meeting of the Japan Inst. Metals (2007) pp. 269.
9) B. Sundman, B. Jansson and J.-O. Andersson: CALPHAD **9** (1985) 52.
10) F. Gonzales and M. Rappaz: Metall. Mater. Trans. A **37A** (2006) 2797.
11) T. Ohashi, T. Hiromoto, H. Fujii, Y. Nuri and K. Asano: Tetsu-to-Hagane **62** (1976) 614.